1. Aboubakr BRAHIMI[1], 2. Djallel KERDOUN[1] , 3. Abderraouf BOUMASSATA [2], 4. Kaouthar Lalia DAHMANI [3]

Laboratory of Electrical Engineering of Constantine (LEEC)(1), National Polytechnic School of Constantine LGEPC-Laboratory(2), Laboratory of sustainable development of electrical energy (LDDEE) (3)
ORCID: 1. 0000-0001-8337-9025

doi:10.15199/48.2024.09.07

Enhancing Performance and Power Quality of a Double-Stage Grid-Connected PV Systems Using Advanced Control Techniques and A Dual-Extended Kalman Filter

Abstract. *Integrating renewable energy, particularly photovoltaic (PV) systems, into the power grid presents challenges for system stability and power quality. This study proposes an innovative approach using fuzzy logic control and Lyapunov stability methods for a double-stage grid-connected PV system. A dual extended Kalman filter (DEKF) accurately estimates inverter current, demonstrating improved system stability, robustness against disturbances, and superior transient response compared to conventional PI control. DEKF reduces measurement noise, leading to lower total harmonic distortion (THD) in inverter and grid currents thus improving power quality.*

Streszczenie. *Włączenie energii odnawialnej, w szczególności systemów fotowoltaicznych (PV), do sieci elektroenergetycznej stwarza wyzwania dla stabilności systemu i jakości energii. W niniejszym badaniu zaproponowano innowacyjne podejście wykorzystujące sterowanie logiką rozmytą i metody stabilności Lapunowa dla dwustopniowego systemu fotowoltaicznego podłączonego do sieci. Podwójny rozszerzony filtr Kalmana (DEKF) dokładnie szacuje prąd falownika, wykazując lepszą stabilność systemu, odporność na zakłócenia i doskonałą reakcję na stany przejściowe w porównaniu z konwencjonalnym sterowaniem PI. DEKF redukuje szumy pomiarowe, prowadząc do niższych całkowitych zniekształceń harmonicznych (THD) w prądach falownika i sieci, poprawiając w ten sposób jakość energii. (**Poprawa wydajności i jakości energii w dwuetapowych systemach fotowoltaicznych podłączonych do sieci przy użyciu zaawansowanych technik sterowania i podwójnego rozszerzonego filtra Kalmana*)

Keywords: Dual extended Kalman filter (DEKF), Fuzzy logic control, Grid-connected PV inverter, Lyapunov stability.
Słowa kluczowe: Podwójny rozszerzony filtr Kalmana (DEKF), sterowanie fuzzy logic, falownik fotowoltaiczny podłączony do sieci, stabilność Lyapunowa.

Introduction

Shifting toward clean renewable energy sources is more important now than ever due to the rise in energy consumption, which relies primarily on fossil fuels leading to more greenhouse gas emissions, photovoltaic is one of the promising types of renewable energy sources due to its abundance, however, integrating it into the existing power grid imposes different challenges including improvement in power quality, overall system stability, compliance with grid requirements and efficiency.[1] There is more than one aspect in which the performance of the PV grid-integrated systems can be improved, from MPPT techniques to power electronic design and control[2], in particular the control of the grid-tied inverter, which plays an important role in the overall performance of the system and the quality of the injected power. Integrating PV systems into the grid is done using either a single-stage configuration where the PV panel is directly connected to the inverter[3], or a double-stage configuration where the PV panel is connected to a DC-to-DC converter which is then fed into the inverter[4], the DC-to-DC converter is controlled by an MPPT algorithm to achieve maximum power extraction, in[5] different types of MPPT techniques are listed. The current control of the inverter can be implemented in a synchronous dq0 reference frame (SRF), stationary αβ0 reference frame, or in the natural abc reference frame.[6]

Several current control techniques used for grid-integrated inverters are present in the existing literature, in[7] fuzzy PI, and fuzzy-sliding mode controller were designed, similarly, a PSO adaptive PI and PR controller were designed in[8], all the above controllers are considered as adaptive control which has its advantages and its shortcomings such as the need for accurate system identification and modeling to estimate the system parameters, adaptation phase which can slow the dynamic response of the system, sensitivity to measurement noise and disturbances. Hysteresis current control is implemented in[9], [10],[11], [12] Hysteresis current control can induce switching losses and harmonic distortions, also lacks precision and shows a sensitivity to noisy measurements, Model Predictive Control (MPC), Sliding Mode Control and PI control were studied and compared in [13] and found that the NPC method is superior and also listed the limits of each controller, the NPC method requires precise modeling of the system and a large computational effort, the PI controller used in[14], [15], [16],[17]can be slow and sensitive to system parameter variation, disturbances, nonlinearities in the system, and measurement noise, in[18] recurrent neural network (RNN) based current control was proposed, learning based intelligent control may be slow due to the learning phase and faster response is key in current control.

Measurement noise can degrade the performance of feedback control by introducing inaccurate measurement leading to reduced stability and inaccurate error tracking[19], [20] Filtering the measured signal is one of the methods used to mitigate the measurement noise, using traditional low pass filters can introduce a larger time delay in the filtered signal, using Kalman filter(KF) or extended Kalman filter (EKF) is a better option, and is used in various applications[21]–[24].

Simple controllers are easy to design and implement but they lack certain performance factors, on the other hand,

overly complex controllers can be difficult to design and implement or heavily demanding on computational power. Measurement noise seems to have a negative effect on the performance of the controller especially in higher gain controllers, and the mentioned studies did not consider the effect of the measurement noise, in this context, this study was conducted to focus on the AC side control of a double-stage grid-connected PV system, the main contributions of the study are:

- Designing a current controller for the inverter using the Lyapunov stability approach implemented in the dq0 frame to ensure the stability of the system and robustness against uncertainties and disturbances.

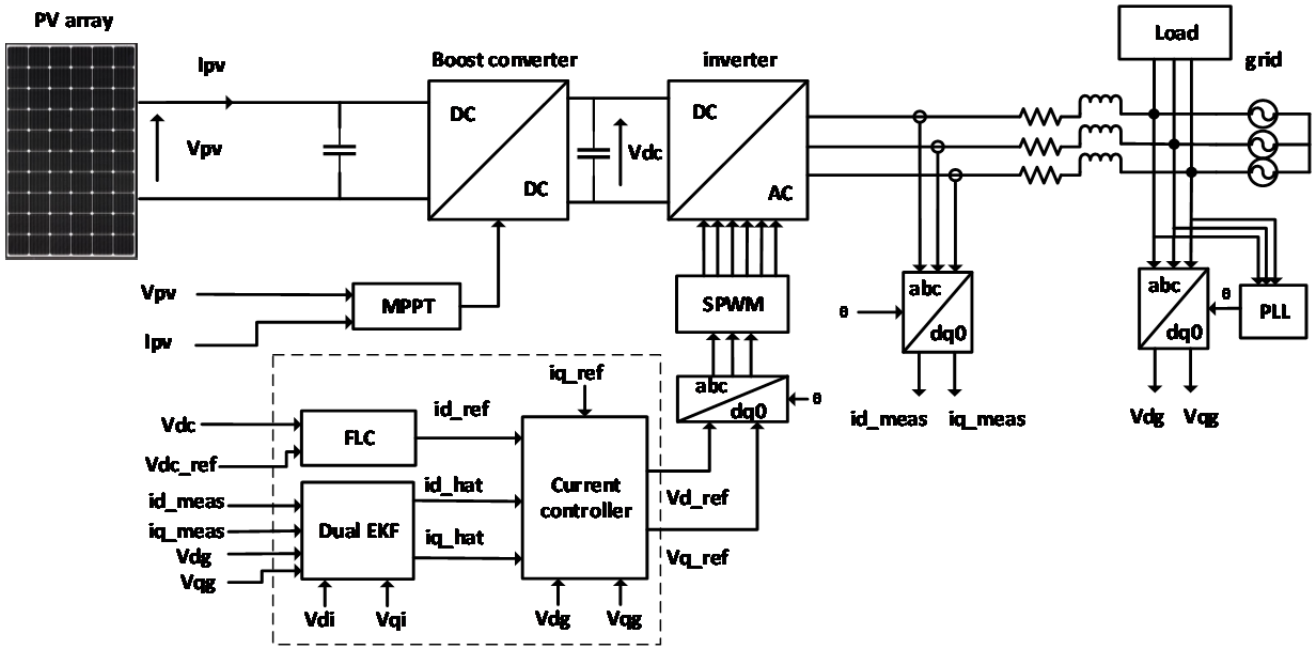

Fig. 1. Double-stage grid-connected PV system with the proposed controller.

• Designing a dual extended Kalman filter for the estimation of the inverter current.
• Designing a fuzzy logic controller for the DC link voltage control.

The article will be structured as follows: In Section 2, an overview of the system is demonstrated, Section 3 contains the modeling of the voltage source inverter in the dq0 reference frame, followed by the design of the dual extended Kalman filter in Section 4, in Section 5 the fuzzy logic controller is designed and the Lyapunov based current control is addressed in Section 6, the results and discussion are mentioned in Section 7, and finely a conclusion is derived.

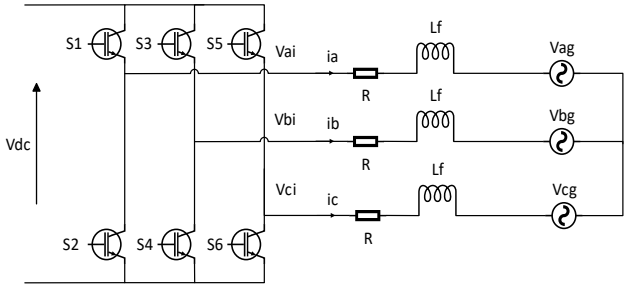

Fig. 2. The circuit of the grid-connected three-phase voltage source inverter.

Overview of the system

A grid-connected PV system in a double-stage configuration shown in Fig (1) is studied in this article, the first stage consists of a PV array connected to a DC-to-DC boost converter that is controlled directly by an MPPT controller, in this case, a commonly used perturb and observe (P&O) algorithm is chosen, this maximizes the power output from the PV array by tracking the maximum power point (MPP) of the solar array, the second stage consists of three phase inverter that converts the DC power present at the DC bus to an AC power that is synchronized with the grid using the phase-locked loop technique(PLL), the proposed controller for the inverter is a two loop controller implemented in a synchronous reference frame (SRF), the voltage is controlled using a fuzzy logic controller and the inverter current is controlled using the Lyapunov stability criteria, this guarantees a stable control and the noisy current measurements are taking in consideration and dealt with using a dual extended Kalman filter, the gate signals for the inverter switches are generated using sinusoidal pulse width modulation technique (SPWM).

Modeling of the three-phase grid-connected inverter

Represented in Fig (2) is a three-phase voltage source inverter connected to the grid through an inductor filter. By applying Kirchhoff voltage law, we get the following equations:

$$\begin{cases} Va_i = Ri_a + Lf\frac{di_a}{dt} + Va_g \\ Vb_i = Ri_b + Lf\frac{di_b}{dt} + Vb_g \\ Vc_i = Ri_c + Lf\frac{di_c}{dt} + Vc_g \end{cases} \quad (1)$$

where Lf and R are the filter inductance and resistance respectively. The inverter control will be implemented in the dq0 synchronous reference frame there for park transformation is needed, park transformation and its inverse are defined as follows:

$$P(\theta) = \frac{2}{3}\begin{bmatrix} \cos(\theta) & \cos(\theta-\frac{2\pi}{3}) & \cos(\theta+\frac{2\pi}{3}) \\ -\sin(\theta) & -\sin(\theta-\frac{2\pi}{3}) & -\sin(\theta+\frac{2\pi}{3}) \\ \frac{1}{2} & \frac{1}{2} & \frac{1}{2} \end{bmatrix} \quad (2)$$

$$P(\theta)^{-1} = \frac{2}{3}\begin{bmatrix} \cos(\theta) & -\sin(\theta) & 1 \\ \cos(\theta-\frac{2\pi}{3}) & -\sin(\theta-\frac{2\pi}{3}) & 1 \\ \cos(\theta+\frac{2\pi}{3}) & -\sin(\theta+\frac{2\pi}{3}) & 1 \end{bmatrix} \quad (3)$$

where θ is the reference angle that will be extracted from the measured grid voltages using 3Ø phase-locked loop, by applying park transformation, equations (1) can be converted to a dq0 synchronous reference frame as follows:

$$Vd_i = R\,id + Lf\frac{di_d}{dt} - \omega\,Lf\,iq + Vd_g \quad (4)$$

$$Vq_i = R\,iq + Lf\frac{di_q}{dt} + \omega\,Lf\,id + Vq_g \quad (5)$$

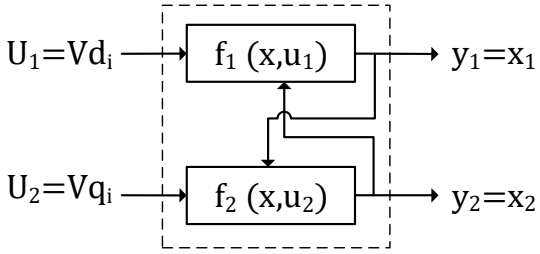

Fig. 3. Block diagram of the system model

The model of our system can be represented in state space format by choosing the state vector to be $x = [x_1 \quad x_2]^T$ where $x_1$is id and x_2 is iq and $y = [y_1 \quad y_2]^T$ is the measurement vector, and the resulting model illustrated in Fig (3) is a multi-input multi-output (MIMO) system.

(6) $$\begin{bmatrix}\dot{x}_1\\ \dot{x}_2\end{bmatrix} = \begin{bmatrix}\frac{R}{Lf} & \omega\\ -\omega & \frac{R}{Lf}\end{bmatrix}\begin{bmatrix}x_1\\ x_2\end{bmatrix} + \frac{1}{Lf}\begin{bmatrix}Vd_i\\ Vq_i\end{bmatrix} + \frac{1}{Lf}\begin{bmatrix}Vd_g\\ Vq_g\end{bmatrix}$$

(7) $$\begin{bmatrix}y_1\\ y_2\end{bmatrix} = \begin{bmatrix}1 & 0\\ 0 & 1\end{bmatrix}\begin{bmatrix}x_1\\ x_2\end{bmatrix}$$

Dual extended Kalman filter design

System state estimation is done in discrete time, for that the system model is described as follows:

(8) $$x_k = f(x_{k-1}, u_{k-1}) + w_k$$

(9) $$y_k = g(x_k) + v_k$$

With f representing the nonlinear equations of the system and g representing the measurement (possibly nonlinear) equation, w_{k-1}~$N(0, Q_{k-1})$ and v_k~$N(0, R_k)$ are process noise and measurement noise respectively. The EKF uses Taylor expansion on the nonlinear system near the filtering point and takes the first order of the series which is the Jacobian matrix, thus the system becomes linear and the basic Kalman filter is applied, the Jacobian matrices for the state transition function and the measurement function are calculated as follows:

(10) $$A_{k-1} = \frac{\partial f(x,k-1)}{\partial x_{k-1}}\Big|_{\hat{x}_{k-1}}$$

(11) $$C_k = \frac{\partial g(x,k)}{\partial x_k}\Big|_{\hat{x}_k}$$

The two main steps in extended Kalman filtering are time update and measurement update:

- time update is where the values of the state variables and error covariance matrix are calculated:

(12) $$\hat{x}_k^- = f(\hat{x}_{k-1}, k-1)$$

(13) $$P_k^- = A_{k-1}P_{k-1}A^T{}_{k-1} + Q_{k-1}$$

- Measurement update: is the estimation based on the Kalman gain and the new state variables:

(14) $$Kf_k = P_k^- C_k^T [C_k P_k^- C_k^T + R_k]^{-1}$$

(15) $$\hat{x}_k = \hat{x}_k^- + Kf_k(y_k - C_k\hat{x}_k^-)$$

(16) $$P_k = [I - Kf_k C_k]P_k^-$$

Kf_k is the Kalman filter gain, $P_k$is the error variance matrix estimation and I is the identity matrix.

As mentioned previously we have a MIMO system that has two separate control inputs and outputs, and since the states of the system are coupled, meaning that each state estimation depends on the other state, for that a dual EKF is constructed to simultaneously estimate the system's states as shown in Fig (4), the dual EKF will be applied to the following system:

(17) $$\begin{bmatrix}x_{1_k}\\ x_{2_k}\end{bmatrix} = \begin{bmatrix}f_1(x_{k-1}, u_{1_{k-1}})\\ f_2(x_{k-1}, u_{2_{k-1}})\end{bmatrix} + \begin{bmatrix}w_k\\ w_k\end{bmatrix}$$

(18) $$\begin{bmatrix}y_{1_k}\\ y_{2_k}\end{bmatrix} = \begin{bmatrix}g_1(x_k)\\ g_2(x_k)\end{bmatrix} + \begin{bmatrix}v_k\\ v_k\end{bmatrix}$$

The Jacobian matrices are:

(19) $$A_{1_{k-1}} = \frac{\partial f_1(x,k-1)}{\partial x_{k-1}}\Big|_{\hat{x}_{k-1}} = \begin{bmatrix}\frac{\partial f_1(x,k-1)}{\partial x_{1_{k-1}}} & \frac{\partial f_1(x,k-1)}{\partial x_{2_{k-1}}}\end{bmatrix} = \begin{bmatrix}\frac{R}{Lf} & \omega\end{bmatrix}$$

(20) $$A_{2_{k-1}} = \frac{\partial f_2(x,k-1)}{\partial x_{k-1}}\Big|_{\hat{x}_{k-1}} = \begin{bmatrix}\frac{\partial f_2(x,k-1)}{\partial x_{1_{k-1}}} & \frac{\partial f_2(x,k-1)}{\partial x_{2_{k-1}}}\end{bmatrix} = \begin{bmatrix}-\omega & \frac{R}{Lf}\end{bmatrix}$$

(21) $$C_{1_k} = \frac{\partial g_1(x,k)}{\partial x_k}\Big|_{\hat{x}_k} = \begin{bmatrix}\frac{\partial g_1(x,k-1)}{\partial x_{1_{k-1}}} & \frac{\partial g_1(x,k-1)}{\partial x_{2_{k-1}}}\end{bmatrix} = [1 \quad 0]$$

(22) $$C_{2_k} = \frac{\partial g_2(x,k)}{\partial x_k}\Big|_{\hat{x}_k} = \begin{bmatrix}\frac{\partial g_2(x,k-1)}{\partial x_{1_{k-1}}} & \frac{\partial g_2(x,k-1)}{\partial x_{2_{k-1}}}\end{bmatrix} = [0 \quad 1]$$

The DEKF algorithm is as follows:

1. Initializing state parameters:

$\hat{x}_1(0)$, $P_{x_1}(0)$; $\hat{x}_2(0)$, $P_{x_2}(0)$

2. Time update for the first state filter:

(23) $$\hat{x}_{1_k}^- = f_1(\hat{x}_{k-1}, k-1)$$

(24) $$P_{1_k}^- = A_{1_{k-1}}p_{1_{k-1}}A_{1_{k-1}}^T + Q_{k-1}$$

3. Time update for the second state filter:

(25) $$\hat{x}_{2_k}^- = f_2(\hat{x}_{k-1}, k-1)$$

(26) $$P_{2_k}^- = A_{2_{k-1}}p_{2_{k-1}}A_{2_{k-1}}^T + Q_{k-1}$$

4. Measurement update for the first state filter:

(27) $$Kf_{1_k} = P_{1_k}^- C_{1_k}^T [C_{1_k}P_{1_k}^- C_{1_k}^T + R_k]^{-1}$$

(28) $$\hat{x}_{1_k} = \hat{x}_{1_k}^- + Kf_{1_k}(y_{1_k} - C_{1_k}\hat{x}_k^-)$$

(29) $$p_{1_k} = [I - Kf_1 C_{1_k}]p_{1_k}^-$$

5. Measurement update for the second state filter:

(30) $$Kf_{2_k} = P_{2_k}^- C_{2_k}^T [C_{2_k}P_{2_k}^- C_{2_k}^T + R_k]^{-1}$$

(31) $$\hat{x}_{2_k} = \hat{x}_{2_k}^- + Kf_{2_k}(y_{2_k} - C_{2_k}\hat{x}_k^-)$$

(32) $$p_{1_k} = [I - Kf_1 C_{2_k}]p_{2_k}^-$$

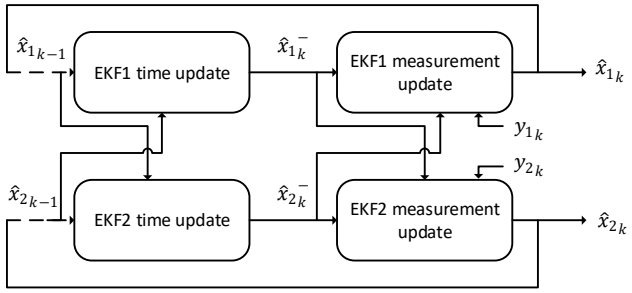

Fig. 4. Block diagram of the Dual extended Kalman filter.

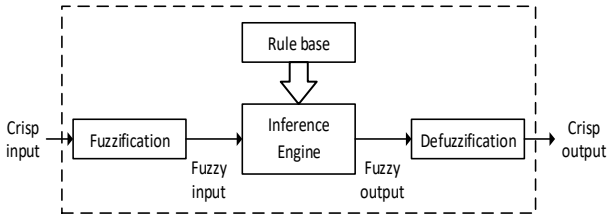

Fig. 5. Structure of a fuzzy logic controller.

Fuzzy logic Voltage control

The proposed controller consists of a two-loop control method, where the first or outer loop is for voltage control and the second or inter loop is for current control, the purpose of the voltage controller is to regulate the DC bus voltage that feeds the inverter to a reference value and outputs a reference current that will be used as input for the current controller, for that, a fuzzy logic controller is designed. The fuzzy logic controller is a type of nonlinear control that is based on human knowledge about the behavior of the system to set rules and make decisions to generate a control signal, unlike traditional control systems that depend on precise mathematical models and crisp logic, fuzzy logic control does not rely on a precise

mathematical model of the system and it is robust in dealing with uncertainties and nonlinearities, Fig (5) shows a diagram illustrating the components of the FLC which are:

Table 1. the fuzzy rules

		Error				
		NB	NS	ZE	PS	PB
ΔError	NB	PB	PB	PS	PS	ZE
	NS	PB	PS	PS	ZE	NS
	ZE	PS	PS	ZE	NS	NS
	PS	PS	ZE	NS	NS	PS
	PB	ZE	NS	NS	PS	PS

• Fuzzification: This step includes converting the crisp inputs provided by measurement into fuzzy sets using membership functions, Linguistic variables such as negative small (NS) and positive big (PB) are used to represent membership functions of each fuzzy set.
• Rule Base: The rule base covers a set of fuzzy rules that define the relationship between the fuzzy input variables and fuzzy output variables, these rules are expressed in IF-THEN format. For example, "IF error is PB AND rate of change in error is PB THEN decrease the control parameter."
• Inference Engine: It applies the fuzzy rules to the fuzzified input variables to determine the appropriate output. The degree to which each rule is satisfied is calculated based on the membership degrees of the input variables, Mamdani or Sugeno methods are often used as an inference engine.
• Defuzzification: In this stage, the fuzzy output is converted into a crisp output value that can be used to control the system using one of these methods: Centre of Gravity Method, Bisector of Area Method, and Mean of minimum Method.

The fuzzy sets of the inputs (error and change in error) and the output (change in the reference current) are composed of five membership functions as shown in Fig (6) and identified using the following linguistic terms: negative big (NB), negative small (NS), zero (ZE), positive small (PS), and positive big (PB), and the rules are presented in Table. 1. The fuzzy rules and membership functions need to be designed and optimized to achieve the desired performance.

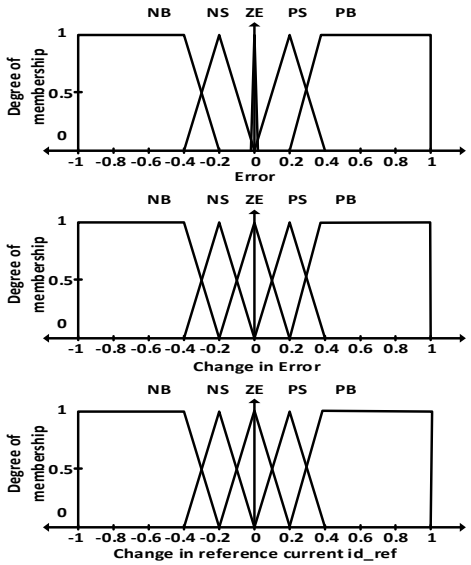

Fig. 6. Membership function design for the fuzzy logic controller.

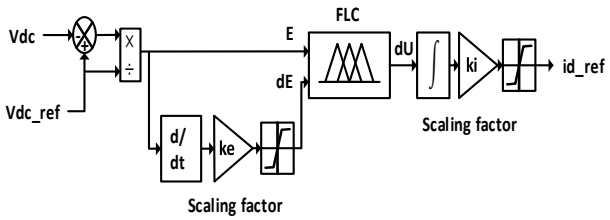

Fig. 7. Block diagram of the voltage controller using fuzzy logic control.

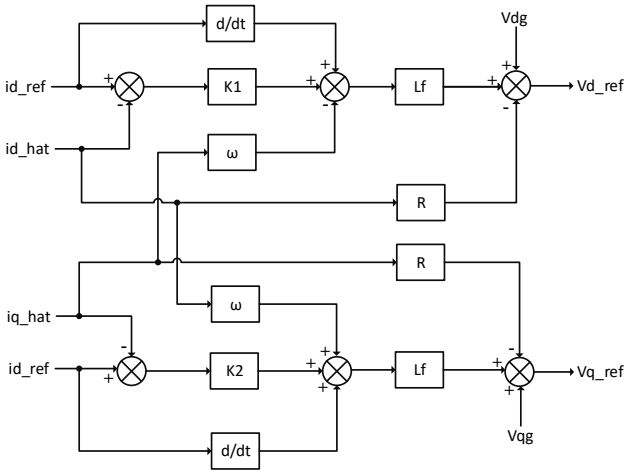

Fig. 8. Block diagram of the current controller.

Current controller design based on the Lyapunov stability approach

The objective of the controller is to make the errors tend to zero in finite time and ensure the system stability, Taking the errors to be the difference between the reference values and the estimated values as:

(33) $$\varepsilon_1 = id_{ref} - \widehat{id}$$

(34) $$\varepsilon_2 = iq_{ref} - \widehat{iq}$$

The derivatives of the errors are:

(35) $$\dot{\varepsilon}_1 = \dot{id}_{ref} - \dot{\widehat{id}}$$

(36) $$\dot{\varepsilon}_2 = \dot{iq}_{ref} - \dot{\widehat{iq}}$$

By substituting $\dot{\widehat{id}}$ and $\dot{\widehat{iq}}$ with their values, we get:

(37) $$\dot{\varepsilon}_1 = \dot{id}_{ref} - \frac{R}{Lf}\widehat{id} - \omega\,\widehat{iq} - \frac{v_d}{Lf} + \frac{vd_g}{Lf}$$

(38) $$\dot{\varepsilon}_2 = \dot{iq}_{ref} - \frac{R}{Lf}\widehat{iq} + \omega\,\widehat{id} - \frac{v_q}{Lf} + \frac{vq_g}{Lf}$$

To analyze the system stability, we consider the following Lyapunov function candidate:

(39) $$V = \frac{1}{2}{\varepsilon_1}^2 + \frac{1}{2}{\varepsilon_2}^2$$

The derivative of the Lyapunov function is:

(40) $$\dot{V} = \varepsilon_1\dot{\varepsilon}_1 + \varepsilon_2\dot{\varepsilon}_2$$

(41) $$\dot{V} = \varepsilon_1\left[\dot{id}_{ref} - \frac{R}{Lf}\widehat{id} - \omega\,\widehat{iq} - \frac{v_d}{Lf} + \frac{vd_g}{Lf}\right] + \varepsilon_2\left[\dot{iq}_{ref} - \frac{R}{Lf}\widehat{iq} + \omega\,\widehat{id} - \frac{v_q}{Lf} + \frac{vq_g}{Lf}\right]$$

For the system to be stable we have to set the control gains such that the derivative of the Lyapunov function becomes negative $\dot{V} < 0$ for that we choose:

(42) $$\dot{\varepsilon}_1 = -k_1\varepsilon_1$$

(43) $$\dot{\varepsilon}_2 = -k_2\varepsilon_2$$

With k_1 and k_2 being positive

(44) $$-k_1\varepsilon_1 = \dot{id}_{ref} - \frac{R}{Lf}\widehat{id} - \omega\,\widehat{iq} - \frac{v_d}{Lf} + \frac{vd_g}{Lf}$$

(45) $$-k_2\varepsilon_2 = \dot{iq}_{ref} - \frac{R}{Lf}\widehat{iq} + \omega\,\widehat{id} - \frac{v_q}{Lf} + \frac{vq_g}{Lf}$$

The reference voltages for the inverter are then extracted to be:

(46) $$vd_{ref} = Lf\left[k_1\varepsilon_1 + \dot{id}_{ref} - \omega\,\widehat{iq}\right] + vd_g - R\,\widehat{id}$$

(47) $$vq_{ref} = Lf\left[k_2\varepsilon_2 + \dot{iq}_{ref} + \omega\,\widehat{id}\right] + vq_g - R\,\widehat{iq}$$

Simulation results and discussions

The proposed system was modeled and simulated using the MATLAB/Simulink 2021 software with the model specifications listed in Table 2, A series of tests were performed to validate the performance of the proposed controller, throughout these tests the system was exposed to different levels of irradiation from 600 to 1000W/m^2 at 0.08s and down to 800 W/m^2 at 0.12s and a constant load.

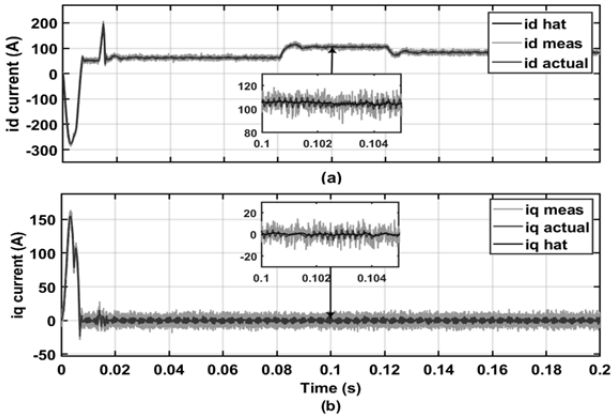

Fig. 9. A comparison between measured, actual, and estimated state values.

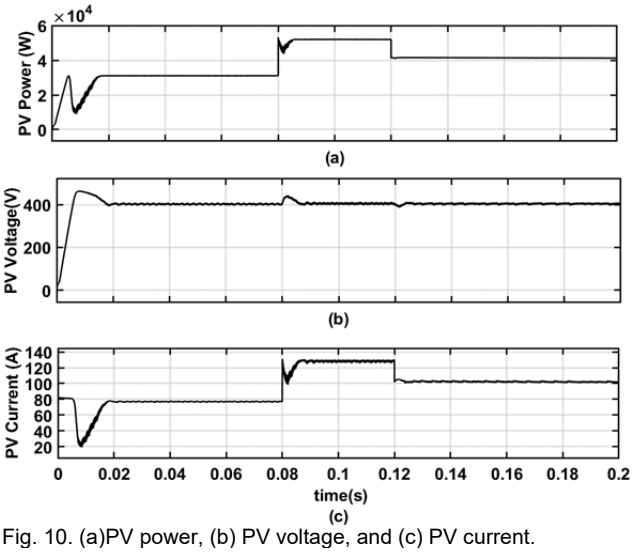

Fig. 10. (a)PV power, (b) PV voltage, and (c) PV current.

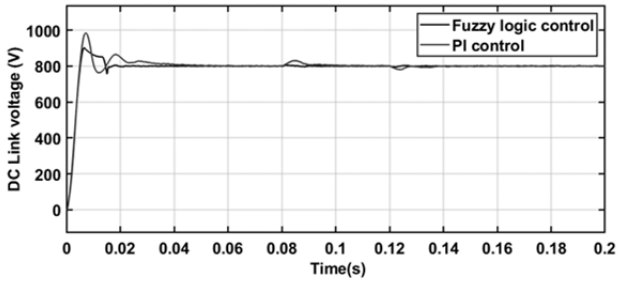

Fig. 11. DC link voltage regulation using fuzzy logic controller compared with PI control.

Table 2. System specifications

parameter	value
Rated PV power	52 Kw
DC link voltage	800 V
DC link capacitor	1000μF
Grid voltage (RMS)/Frequency	400v/50Hz
Load	100 Kw
Filter inductor *Lf*	2mH
Filter inductor resistance *R*	0.01Ω
Inverter switching frequency	50 kHz

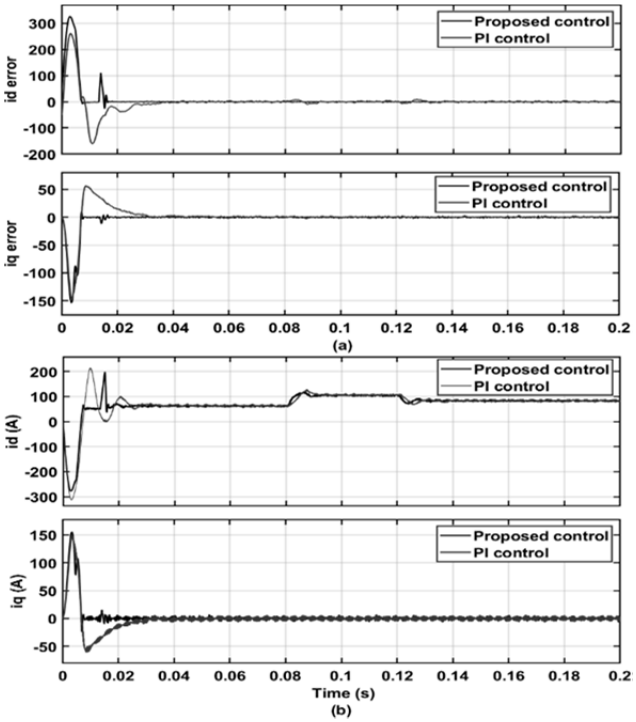

Fig. 12. (a)inverter reference currents tracking error.(b)actual dq inverter currents.

To assess the efficacy of the DEKF, an evaluation of its performance was conducted. This evaluation aimed to validate the accuracy of the estimated state values by comparing them with both the noisy measurements and the actual states. Fig (9) depicts the graphical representation of this comparative analysis. To simulate the realistic conditions encountered in practical situations, Gaussian white noise was intentionally introduced into the clean measurements, thereby generating the measurement noise. This noise addition was performed to mimic the inherent uncertainties and imperfections commonly encountered during real-world data acquisition processes. The obtained results from the evaluation show that the estimated states $\widehat{\imath d}$ and $\widehat{\imath q}$ are a good approximation to the actual states. This observation confirms the effectiveness of the DEKF in mitigating the measurement noise, allowing for the extraction of accurate and reliable state estimations.

Next, the evaluation of the DC side control using the fuzzy logic control was carried out, this evaluation aimed to assess the robustness and effectiveness of the fuzzy logic controller in comparison to the conventional Proportional-Integral (PI). The reference voltage for the DC link was set to 800V while the PI controller parameters were chosen as p=1.5 and I=150. Throughout the evaluation process, it was observed that changes in solar irradiation led to corresponding variations in the output current generated by the photovoltaic (PV) system Fig (10). These changes in output current consequently affected the voltage at the DC link, introducing disturbances into the system. The primary objective was to evaluate how well the fuzzy logic controller and the PI controller responded to these disturbances and the results are presented in Fig (11). The fuzzy logic controller exhibited excellent performance in rejecting the disturbances. Unlike the PI controller, which displayed sensitivity towards the disturbances, the fuzzy logic controller showcased a remarkable capability to reduce the disruptive effects of the variations in solar irradiation. This robustness in disturbance rejection demonstrates the superiority of the fuzzy logic control approach. Moreover, the fuzzy logic controller demonstrated a more favorable

transient response during the initial phase of operation. It exhibited less overshoot, indicating a smoother and more controlled response, and achieved a faster settling time compared to the PI controller. These characteristics highlight the agility and efficiency of the fuzzy logic controller in quickly attaining the desired steady-state conditions, ensuring a more stable and optimized performance

The Lyapunov-based controller is then looked into and compared to PI current control strategy, the parameters of the proposed controller are selected as k1=k2=6000 based on the desired performance. The primary objective of the Lyapunov-based controller is to achieve zero steady-state error, ensuring precise tracking of the desired reference signal, while simultaneously guaranteeing system stability. It is important to note that both the Lyapunov-based controller and the PI controller achieve the desired zero steady-state error, However, the comparative analysis of the results from Fig (12) reveals notable distinctions between the two control strategies, the proposed Lyapunov-based controller exhibits a faster time response, manifesting in a significantly reduced settling time. This indicates its ability to more rapidly attain the desired reference signal, thereby improving the overall system's dynamic performance.

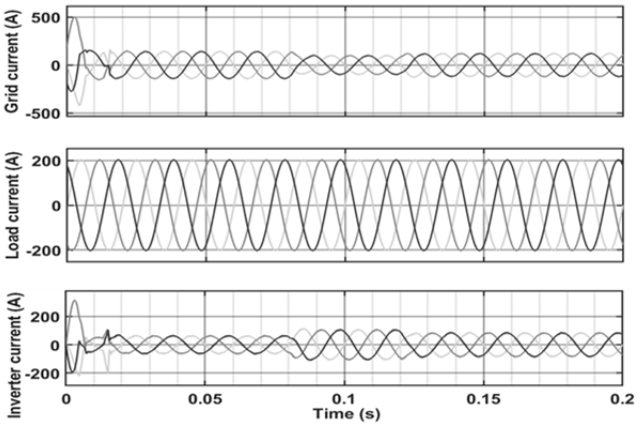

Fig. 13. grid, load, and inverter currents (a) Proposed control+DEKF, (b) PI control+DEKF.

Furthermore, the Lyapunov-based controller demonstrates enhanced stability characteristics compared to the PI controller. The proposed controller ensures robust stability, even in the presence of uncertainties or disturbances. This increased stability is reflected in a reduced oscillation and a more consistent response.

The quality of the injected power was looked into by analyzing the THD levels of the inverter current and grid current using PI control, and the proposed controller Fig (13.14), and the results were summarized in Table.3. The analyses of the THD levels show the impact of considering the measurement noise and the effectiveness of the DEKF in reducing the THD levels in PI-controlled inverter current and grid current by 8.53% and 8.45% respectively, and a decrease in THD levels of the Lyapunov based control of the inverter and grid current by 9.09% and 8.86% respectively thus improving the quality of the injected power.

Table 3. THD levels of inverter current and grid current.

Control method	Inverter current DHT	Grid current DHT
PI control	4.10%	2.84%
Proposed control	4.07%	2.82%
PI control+DEKF	3.75%	2.60%
Proposed control+DEKF	3.70%	2.57%

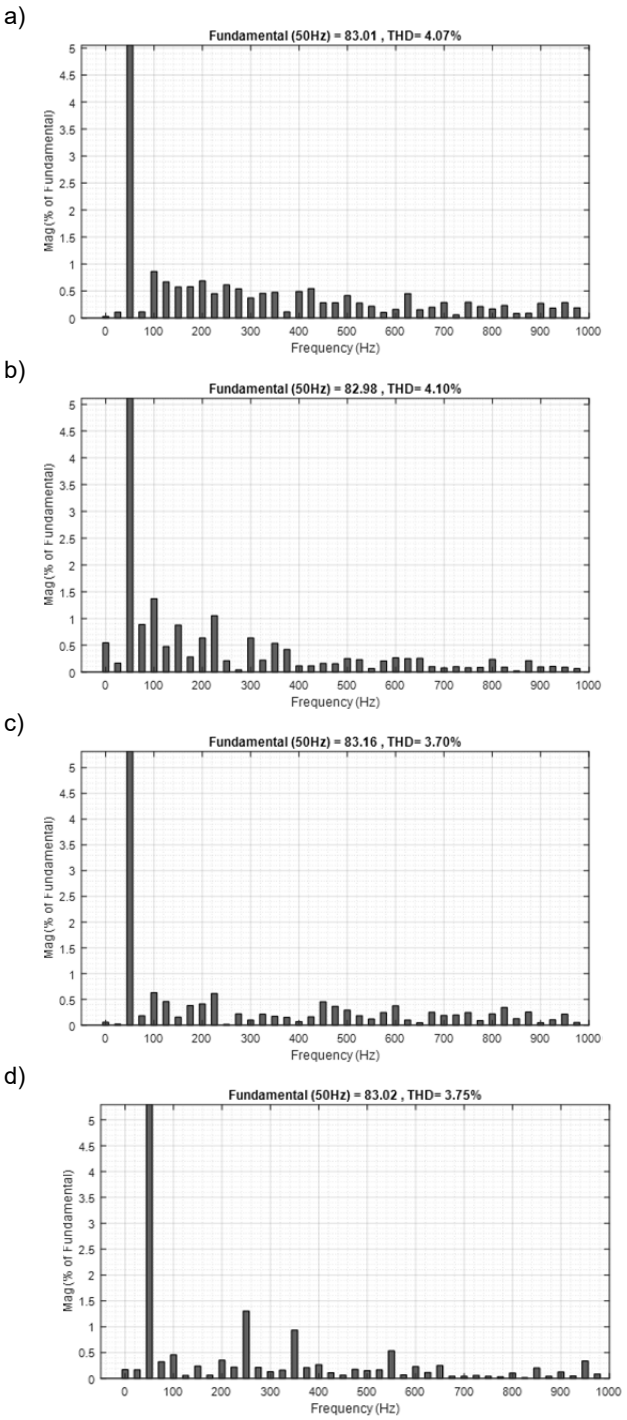

Fig. 14. Inverter current THD (a)proposed control, (b) PI control, (c) Proposed control+DEKF, (d) PI control+DEKF.

conclusion

In conclusion, this research focused on improving the performance and power quality of a grid-connected PV system. The study emphasized the significance of advanced control techniques for power electronics converters to enhance the system's efficiency and reliability. Specifically, the research addressed the AC side control of a double-stage grid-connected PV system, employing a fuzzy logic controller for the DC link and a Lyapunov stability approach for the inverter's current control. The results demonstrated the effectiveness of these control methods in stabilizing the DC link voltage, ensuring system stability, and robustness against uncertainties and disturbances. The impact of measurement noise on power

quality was observed in the form of increased total harmonic distortion (THD) levels in both grid and inverter currents, To mitigate this issue, a dual-extended Kalman filter was designed and successfully applied, effectively eliminating measurement noise leading to a significant reduction in THD levels. This resulted in an enhanced power quality for the grid-connected PV system.

***Authors**: Mr. Aboubakr Brahimi, Laboratory of Electrical Engineering of Constantine (LEEC), RN79, Constantine 25000, Algeria, Email: aboubakr.brahimi@doc.umc.edu.dz; Prof. dr Djallel Kerdoun, Laboratory of Electrical Engineering of Constantine, RN79, Constantine 25000, Algeria, Email: kerdoun.djallel@umc.edu.dz; Prof. dr Abderraouf Boumassata, National Polytechnic School of Constantine LGEPC-Laboratory, BP 75, A, Nouvelle ville RP, Constantine, Email: a boumassata@umc.edu.dz; Miss. Kaouthar Lalia Dahmani, Laboratory of sustainable development of electrical energy (LDDEE) MB 31000, Algeria, Email: Kaoutharlalia.dahmani@univ-usto.dz*

REFERENCES

[1] M. Morey, N. Gupta, M. M. Garg, and A. Kumar, “A comprehensive review of grid-connected solar photovoltaic system: Architecture, control, and ancillary services,” Renewable Energy Focus, vol. 45, pp. 307–330, 2023. doi: 10.1016/j.ref.2023.04.009.

[2] R. Panigrahi, S. K. Mishra, S. C. Srivastava, A. K. Srivastava, and N. N. Schulz, “Grid Integration of Small-Scale Photovoltaic Systems in Secondary Distribution Network—A Review,” IEEE Trans Ind Appl, vol. 56, no. 3, pp. 3178–3195, 2020, doi: 10.1109/TIA.2020.2979789.

[3] K. Kumari and A. K. Jain, “Performance Assessment of Three-Phase NPC-Based Grid Integrated Single-Stage Solar PV System With Reduced DC Bus Capacitor,” IEEE Transactions on Industrial Electronics, vol. 70, no. 4, pp. 3773–3781, 2023, doi: 10.1109/TIE.2022.3179545.

[4] N. Tak, S. K. Chattopadhyay, and C. Chakraborty, “Single-Sourced Double-Stage Multilevel Inverter for Grid-Connected Solar PV Systems,” IEEE Open Journal of the Industrial Electronics Society, vol. 3, pp. 561–581, 2022, doi: 10.1109/OJIES.2022.3206352.

[5] A. Nadeem and A. Hussain, “A comprehensive review of global maximum power point tracking algorithms for photovoltaic systems,” Energy Systems, vol. 14, no. 2, pp. 293–334, 2023, doi: 10.1007/s12667-021-00476-2.

[6] I. D. L. Costa, D. I. Brandao, L. M. Junior, M. G. Simões, and L. M. F. Morais, “Analysis of stationary-and synchronous-reference frames for three-phase three-wire grid-connected converter AC current regulators,” Energies (Basel), vol. 14, no. 24, 2021, doi: 10.3390/en14248348.

[7] K. Zeb et al., “High-performance and Multi-functional Control of Transformerless Single-phase Smart Inverter for Grid-connected PV System,” Journal of Modern Power Systems and Clean Energy, vol. 9, no. 6, pp. 1386–1394, Nov. 2021, doi: 10.35833/MPCE.2019.000331.

[8] H. I. Alkhammash et al., “Optimization of Proportional Resonant and Proportional Integral Controls Using Particle Swarm Optimization Technique for PV Grid Tied Inverter,” Mathematical Modelling of Engineering Problems, vol. 10, no. 1, pp. 23–30, 2023, doi: 10.18280/MMEP.100103.

[9] P. Pydikalva, S. Natarajan, B. Aljafari, K. Balasubramanian, and S. B. Thanikanti, “PV-Fed Micro-Inverter with Battery Storage for Single Phase Grid Applications,” Electric Power Components and Systems, vol. 51, no. 11, pp. 1051–1074, 2023, doi: 10.1080/15325008.2023.2189758.

[10] Nur Fairuz Mohamed Yusof, D. Ishak, and M. A. A. M. Zainuri, “Modified PQ and Hysteresis Current Control in Grid-Connected Single-Phase Inverter for PV System,” Russian Electrical Engineering, vol. 94, no. 3, pp. 212–221, 2023, doi: 10.3103/S1068371223030136.

[11] S. K. Dash and P. K. Ray, “Power quality improvement utilizing PV fed unified power quality conditioner based on UV-PI and PR-R controller,” CPSS Transactions on Power Electronics and Applications, vol. 3, no. 3, pp. 243–253, 2018, doi: 10.24295/CPSSTPEA.2018.00024.

[12] Z. Yao, Y. Zhang, and X. Hu, “Transformerless Grid-Connected PV Inverter Without Common Mode Leakage Current and Shoot-Through Problems,” IEEE Transactions on Circuits and Systems II: Express Briefs, vol. 67, no. 12, pp. 3257–3261, 2020, doi: 10.1109/TCSII.2020.2990447.

[13] E. Macit and A. M. Vural, “Modelling and Simulation of 1 MW Grid-Connected PV System Regulated by Sliding Mode Control, Model Predictive Control and PI Control,” Gazi University Journal of Science, vol. 35, no. 4, pp. 1433–1452, 2022, doi: 10.35378/gujs.899799.

[14] R. Kadri, J.-P. Gaubert, and G. Champenois, “An Improved Maximum Power Point Tracking for Photovoltaic Grid-Connected Inverter Based on Voltage-Oriented Control,” IEEE Transactions on Industrial Electronics, vol. 58, no. 1, pp. 66–75, 2011, doi: 10.1109/TIE.2010.2044733.

[15] S. Ahmad et al., “Direct Power Control Based on Point of Common Coupling Voltage Modulation for Grid-Tied AC Microgrid PV Inverter,” IEEE Access, vol. 10, pp. 109187–109202, 2022, doi: 10.1109/ACCESS.2022.3213939.

[16] Y. Singh, B. Singh, and S. Mishra, “Control of Multiple SPV Integrated Parallel Inverters for Microgrid Applications,” IEEE Trans Ind Appl, vol. 59, no. 3, pp. 3700–3712, 2023, doi: 10.1109/TIA.2023.3244531.

[17] N. F. Ibrahim, K. Mahmoud, M. Lehtonen, and M. M. F. Darwish, “Comparative Analysis of Three-Phase PV Grid Connected Inverter Current Control Schemes in Unbalanced Grid Conditions,” IEEE Access, vol. 11, pp. 42204–42221, 2023, doi: 10.1109/ACCESS.2023.3270262.

[18] V. N. Kumar, N. Babu P., R. Kiranmayi, P. Siano, and G. Panda, “Improved Power Quality in a Solar PV Plant Integrated Utility Grid by Employing a Novel Adaptive Current Regulator,” IEEE Syst J, vol. 14, no. 3, pp. 4308–4319, 2020, doi: 10.1109/JSYST.2019.2958819.

[19] M. Sadeghighasami, M. Shafieirad, and I. Zamani, “Robust Output Feedback Controller Design Based on Kalman Filter for Switched Positive Discrete-Time Systems,” Circuits Syst Signal Process, 2023, doi: 10.1007/s00034-023-02398-z.

[20] W. Zhu et al., “Using dynamic data reconciliation to improve the performance of PID feedback control systems with Gaussian/non-Gaussian distributed disturbance and measurement noise,” ISA Trans, vol. 137, pp. 544–560, 2023, doi: 10.1016/j.isatra.2023.01.015.

[21] N. Vafamand, M. M. Arefi, M. Shafie-Khah, and J. P. S. Catalão, “Adaptive Optimal Control of Faulty Nonlinear DC Microgrids With Constant Power Loads: Dual-Extended Kalman Filter Approach,” IEEE Trans Ind Appl, vol. 59, no. 1, pp. 513–522, 2023, doi: 10.1109/TIA.2022.3206169.

[22] D. S. Nair, G. Jagadanand, and S. George, “Torque Estimation using Kalman Filter and Extended Kalman Filter Algorithms for a sensorless Direct Torque Controlled BLDC Motor drive: A Comparative Study,” Journal of Electrical Engineering and Technology, vol. 16, no. 5, pp. 2621–2634, 2021, doi: 10.1007/s42835-021-00793-7.

[23] M. P. Belov, A. M. Belov, and N. van Lanh, “Sensorless Vector Control of a Permanent-Magnet Synchronous Motor Based on an Extended Adaptive Kalman Filter,” Russian Electrical Engineering, vol. 93, no. 3, pp. 148–154, 2022, doi: 10.3103/S1068371222030026.

[24] E. Moradi and R. Mohseni, “Parameters estimation of linear frequency modulated signal using Kalman filter and its extended versions,” Signal Image Video Process, vol. 17, no. 2, pp. 553–561, 2023, doi: 10.1007/s11760-022-02260-w.